Supporting Information

Regulating the interfacial electric field of NbP-NbC heterostructures to efficiently inhibit polysulfide shuttling in Li−S batteries

Tao Ren [a], Xinyuan Wang [a], Nannan Wang [a], Dan Huang [a], Yanqiu Zhu [a,b], Pei Kang Shen [a], Jinliang Zhu[a]*

[a] School of Resources, Environment and Materials, Guangxi Key Laboratory of Processing for Non-ferrous Metals and Featured Materials, College of Physics Science and Technology, Guangxi University, Nanning 530004, P. R. China. E-mail: jlzhu@gxu.edu.cn
[b] College of Engineering, Mathematics and Physical Sciences, University of Exeter, Exeter EX4 4QF, UK

Experimental section

Physical characterization

The D/Max-III diffractometer (Rigaku Corporation, Japan; Cu Kα, 30 mA, and 40 kV) was used to analyze the sample diffraction patterns at a scanning speed of 8°/min to obtain information regarding the crystal structure and crystallinity. The microstructural characterizations were evaluated by field emission scanning electron microscopy (SU8220, Hitachi Corp., Japan) and transmission electron microscopy (Tian ETEM G2 80-300, FEI Corp., USA). The S content was measured by a thermogravimetric analyzer (DSC/TGA; Netzsch STA449 F5 Jupiter) at 30–850°C under nitrogen protection. Pore structure analysis and the specific surface area were determined at 77 K on a Micromeritics ASAP 2460 instrument (Micromeritics Co., USA). The surface state and chemical environment of the samples were analyzed by monochrome Al Kα radiation X-ray photoelectron spectroscopy (XPS, ESCALab 250Xi, Thermo Fisher Scientific, USA; Al Kα), and the electrical

conductivity of the samples was assessed by using an ST-2722 semiconductor resistivity tester (Suzhou Jingge Electronic Co., Ltd.).

Adsorption tests and UV-vis spectra

A mixture of sulfur and lithium sulfide (mole ratio: 1:5) was added to 1,2-dimethoxyethane/1,3-dioxolane (DME/DOL, 1:1 v/v) and stirred at 60°C for 24 h to obtain the Li_2S_6 solution. To visually observe polysulfide adsorption, 20 mg of samples of the diverse composites (NbP-NbC/C, NbC/C, and NbP/C) was separately added to 4 mL of Li_2S_6 solution and photographed after 3 h at room temperature. An ultraviolet/visible spectrophotometer (PerkinElmer Lambda 650, USA) was then used to further investigate the adsorption capacity of each composite as well as the UV-vis absorption spectrum.

Electrochemical measurements

The electrochemical activities of the samples were evaluated when used as the cathode in LSBs. The NbP-NbC/C@S, NbC/C@S, and NbP/C@S composite electrodes were used as the cathode, while the anode consisted of a lithium metal sheet, which was used to assemble the coin batteries. The electrolyte of the LSBs was composed of a mixture of DME/DOL with a volume ratio of 1:1 and 1.0 M LiTFSI and 2 wt% $LiNO_3$ as an additive. The batteries were assembled using a button cell (CR 2032) in an argon-shielded glove box.

The cycle and rate performance of the cells were evaluated by galvanostatic charge-discharge tests on a battery testing system (Shenzhen Neware Battery Co., China) at 1.7-2.8 V. The value of 1C was calculated according to the theoretical capacity of sulfur, which is 1675 mAh/g. The cyclic voltammetry (CV) tests were carried out on an IM6 electrochemical workstation (Zahner-Elektrik, Germany) in the potential range of 1.7–2.8 V, with a rate of 0.1 mV/s. Electrochemical impedance spectroscopy (EIS) analysis was performed in the frequency range of 100 kHz to 10 MHz using 5 mV as the voltage amplitude.

Li_2S_6 symmetric cells

First, 0.25 mol/L of Li_2S_6 solution (1:1 v/v DME/DOL solution containing 1.0 M LiTFSI and 1 wt% $LiNO_3$) was used as the electrolyte in the symmetrical cells. Two identical electrodes were assembled into a 2032 cell and the CV curves were obtained at a sweep rate of 1.0 mV/s over a voltage range of −1.0 to 1.0 V.

Li_2S nucleation

First, 0.4 mol/L of Li_2S_8 solution was obtained by stirring Li_2S and S (1:7 molar ratio) in a mixed solvent of DME/DOL (1:1 v/v) containing 1.0 M LiTFSI. Then, 20 μL of Li_2S_8 solution was added to the cathode side and 20 μL of electrolyte (1:1 v/v DME/DOL solution containing 1.0 M LiTFSI) was added to the anode side. The cells were galvanostatically discharged to 2.06 V at 0.112 mA and potentiostatically maintained at 2.05 V.

The galvanostatic intermittent titration (GITT) test

NbP-NbC/C@S was used as the sulfur cathode, with a lithium strip as the anode. A current pulse at 0.05C was utilized for 10 min, followed by 20 min of rest between 1.7 and 2.8 V (vs Li^+/Li). QOCV represented the open-circuit voltage, while CCV represented the closed-circuit voltage.

Three-electrode measurements

The S-shaped linear sweep voltammetry (LSV) curves were obtained by a three-electrode measuring system on an electrochemical workstation (Zahner IM6e, Germany). The working electrode consisted of a rotating disk electrode (RDE) with a glassy carbon electrode. Specifically, 5 mg of electrocatalyst, such as NbP-NbC/C, was dispersed in a solution containing 483 μL of deionized water, 483 μL of isopropanol, and 33 μL of Nafion (5 wt%, DuPont, USA). The resulting mixture was ultrasonicated for 30 min and the obtained slurry was uniformly loaded on the electrode via the drop-casting method. The areal loading of the electrocatalyst on the working electrode was 0.10 mg/cm^2. The electrocatalytic properties were then characterized in electrolytes consisting of 4.0 mM S_8 and 1.0 M LiTFSI dissolved in DME/DOL (1:1, by volume) under the continuous flow of nitrogen. The S_8 reduction

reaction was assessed by LSV at a sweep rate of 5 mV/s from 2.8 to 1.6 V. The Tafel slopes were calculated using the Tafel equation based on the LSV curves.

Density functional theory (DFT) calculations

First-principles calculations were performed based on the density functional theory (DFT) using the Vienna ab initio simulation package (VASP). The exchange-correlation energy was described by the generalized gradient approximation (GGA) with the Perdew-Burke-Ernzerhof (PBE) functional. The plane-wave cut-off energy was set to 500 eV for geometry optimization. Brillouin-zone integration was performed using a Monkhorst–Pack grid of k-point sampling, and the G-centered meshes of 15 × 15 × 1 and 3 × 3 × 1 were used for the unit cell and the 4 × 4 × 1 supercell, respectively. During geometry relaxation, the energy convergence criterion was set to 10^{-5} eV, while for self-consistent field calculations, an energy convergence criterion of 10^{-5} eV was used.

The adsorption energy (E_{ads}) was calculated as follows:

$$E_{ads}=E_{total}-E_{sub}-E_{liPSs},$$

where E_{total} is the total energy of the LiPSs adsorbed systems, E_{sub} and E_{liPSs} are the energy of the substrate and the isolated LiPSs molecule, respectively.

The Gibbs free energy change ΔG of each step was calculated as follows:

$$\Delta G = \Delta E + \Delta ZPE - T\Delta S,$$

where ΔE, ΔZPE, and TΔS represent the changes of the DFT-calculated total energy, zero-point energy (ZPE), and entropic contribution, respectively. The ZPE and entropic contribution were calculated from the vibrational frequencies, and a temperature of 298 K was used.

In situ Raman and XRD measurements

A button cell was installed in a device with a quartz window (Beijing Scistar Technology Co. Ltd., China) to record the in situ Raman spectra in the wavelength range of 50–600 cm^{-1}. The

Raman spectra data were collected every 0.1 V at a current density of 0.2 C during the discharge and charge test, and in situ XRD experiments recorded the 2θ diffraction patterns between 20° and 35° at a current density of 0.2 C.

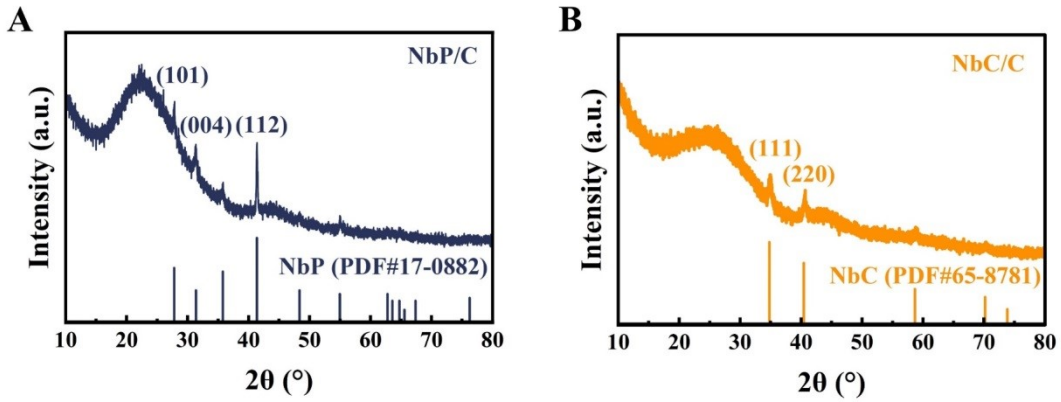

Fig. S1. XRD patterns of NbP/C and NbC/C.

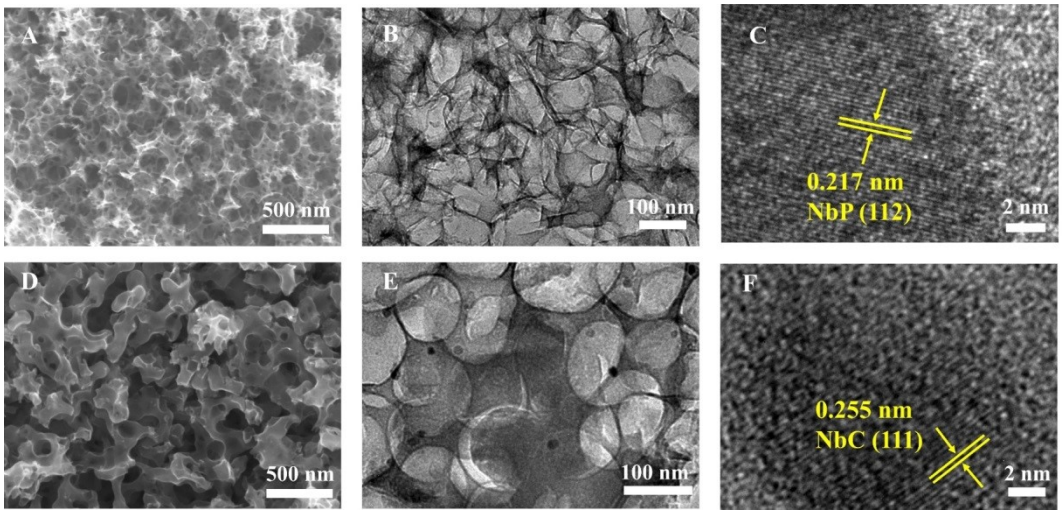

Fig. S2. SEM, TEM, and HRTEM images of (A–C) NbP/C and (D–F) NbC/C.

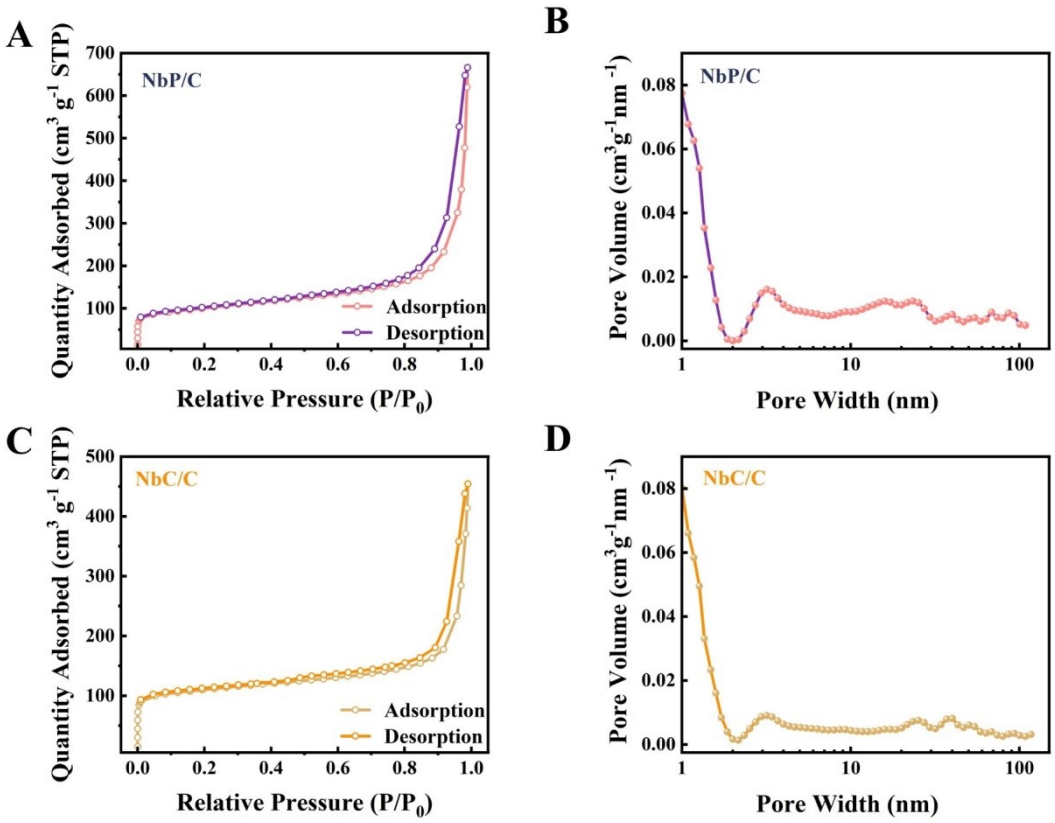

Fig. S3. (A, C) N_2 adsorption-desorption isotherms and (B, D) pore size distribution curves of NbP/C and NbC/C.

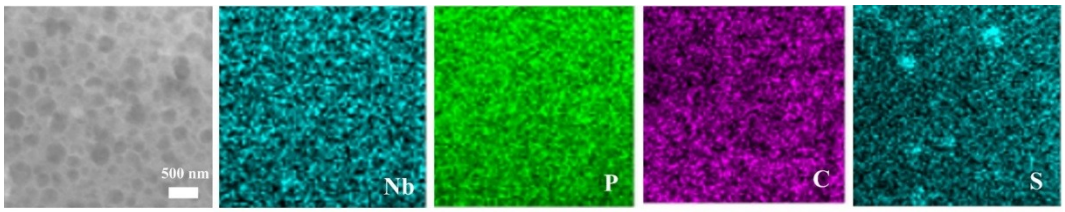

Fig. S4. EDS element distribution mappings of NbP-NbC/C@S.

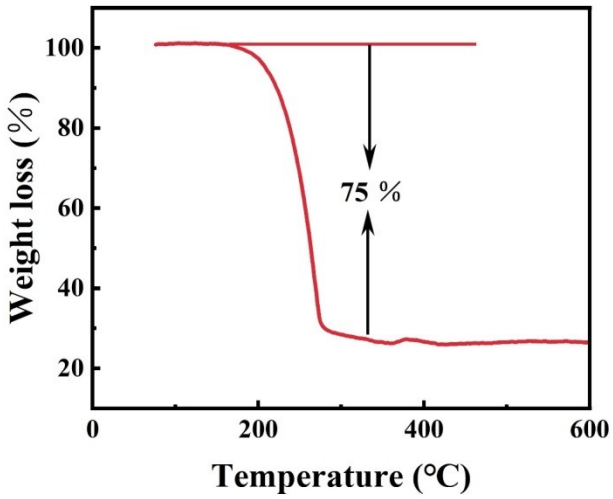

Fig. S5. TG curve of NbP-NbC/C@S.

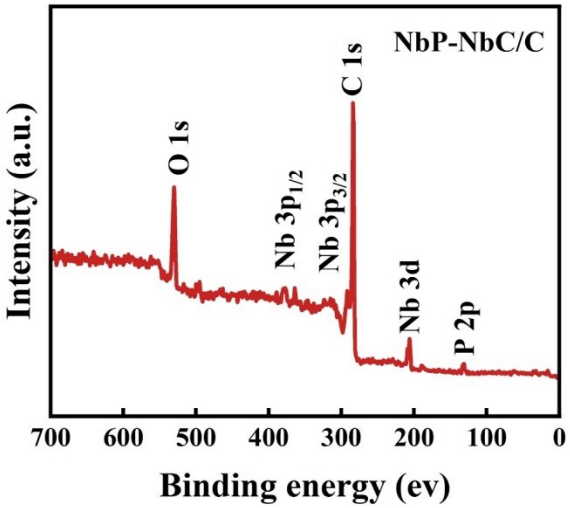

Fig. S6. Survey XPS spectrum of NbP-NbC/C.

Fig. S7. Conductivity of NbP-NbC/C, NbP/C, and NbC/C.

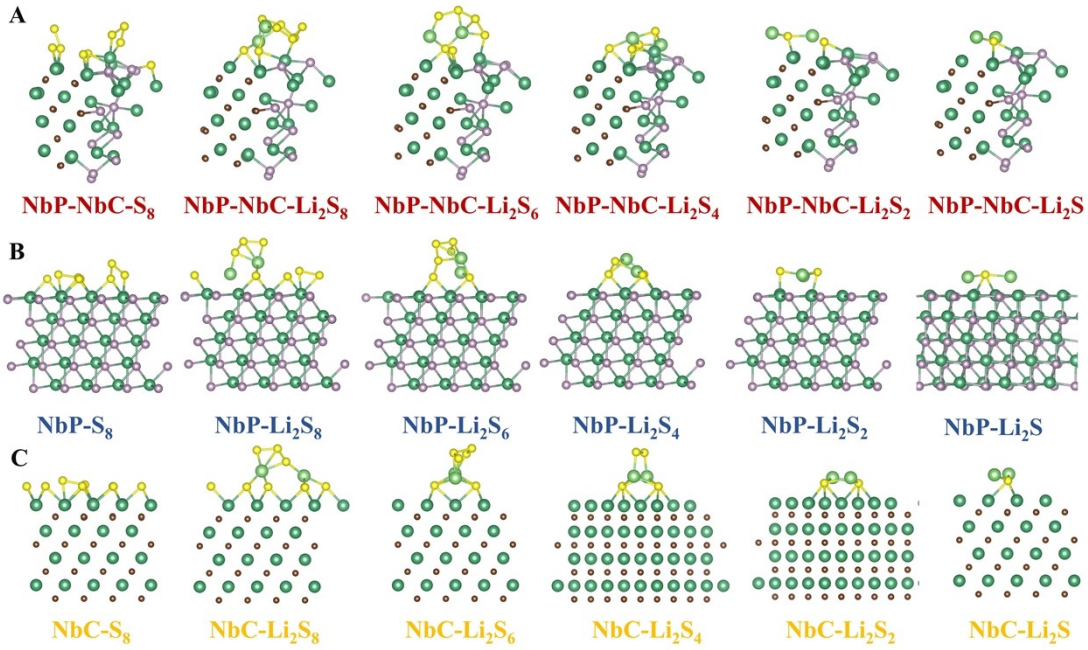

Fig. S8. Optimized conformations and corresponding adsorption energies of LiPS clusters absorbed on the surface of (A) NbP-NbC, (B) NbP, and (C) NbC.

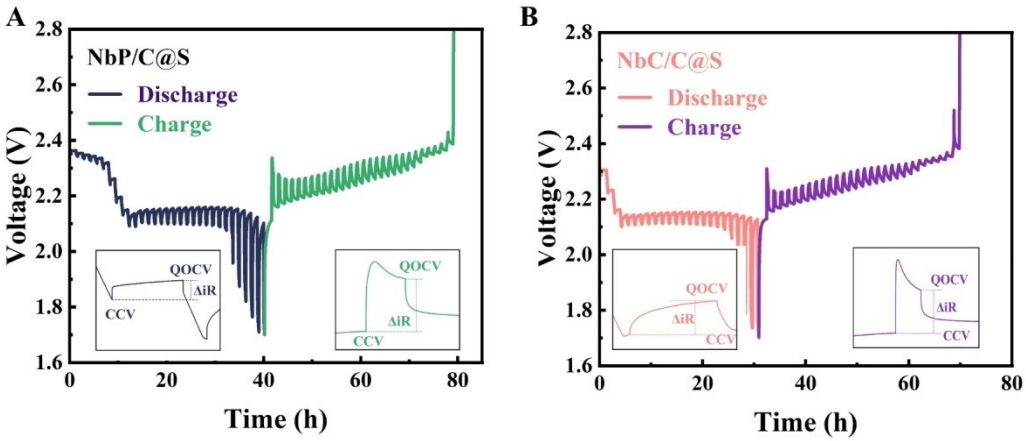

Fig. S9. GITT curves of (A) NbP/C@S and (B) NbC/C@S.

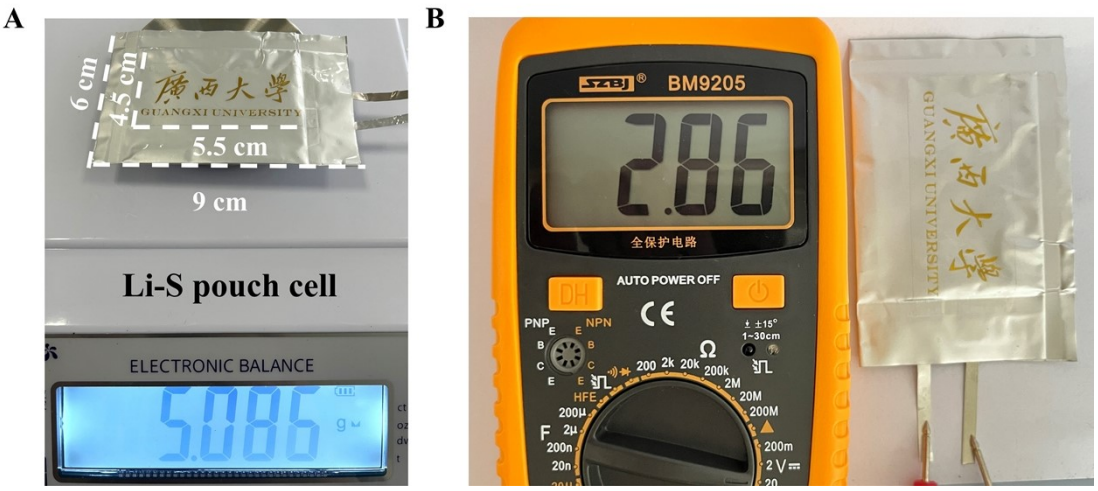

Fig. S10. (A) The main dimensions and weight and (B) the open-circuit voltage of the pouch cell.

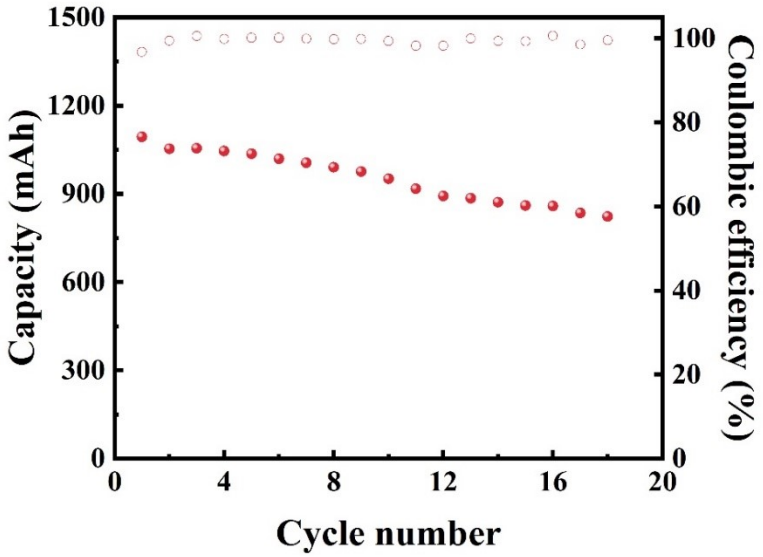

Fig. S11. Cycling performance of the Li-S pouch cell with NbP-NbC/C@S cathodes.

Table S1. Comparison of electrochemical performances among NbP-NbC/C@S and reported electrode materials for Li-S batteries.

Electrode material	**Sulfur loading (mg/cm^2)**	**Current density**	**Cycle number**	**Initial capacity (mAh/g)**	**Ref.**
Sulfur//NbN	1.3	1C	400	847.9	1
Mn_3O_4-MnP_x/C@S	1.5	0.5C	1000	1200	2
S@Zn/SnS_2@NC	1.3–1.5	1C	500	931	3
TSC/NbC-S	1.4–1.6	0.1C	500	937.9	4
Mn/Co-N-C	0.6	2C	1000	816	5
S-V_2O_3/V_8C_7@C@G	1.2–1.5	0.2C	200	1076.9	6
Pt- Nb_2O_5-CNT	1.3	0.2C	100	1283	7
Pt-NbC	1.0	0.2C	100	1382	8
S@Ni-CeO_2-CNF	1.0	0.2C	100	1208.7	9
Nanocrystalline NbC	1.5	0.2C	200	1124.6	10
S/Nb_2O_5/C	1.3	0.2C	100	969	11
S@Nb_2O_5 nanoarrays	1.0–1.2	1C	300	759.6	12
NbN/NG@PP	2.34	0.2C	100	1086	13
MoP-MoO_2/PCNFs	-	1C	400	856.9	14
S@CoFeMnO	-	0.2C	-	1091	15
NbP-NbC/C@S	**1.2**	**0.2C** **2C** **5C**	**250** **1000** **1000**	**1367.9** **879.1** **844.5**	**Our work**

References

1 N. A. X. Shi, B. J. Xi, J. Liu, Z. C. Y. Zhang, N. Song, W. H. Chen, J. K. Feng and S. L. Xiong, *Adv. Funct. Mater.*, 2022, **32**, 2111586.

2 K. Guo, G. Qu, J. Li, H. Xia, W. Yan, J. Fu, P. Yuan and J. Zhang, *Energy Storage Mater.*, 2021, **36**, 496-503.

3 B. Yan, Y. Li, L. Gao, H. Tao, L. Zhang, S. Zhong, X. Li and X. Yang, *Small*, 2022, **18**, 2107727.

4 S. H. Shen, X. H. Xia, Y. Zhong, S. J. Deng, D. Xie, B. Liu, Y. Zhang, G. X. Pan, X. L. Wang and J. P. Tu, *Adv. Mater.*, 2019, **31**, 1900009.

5 S. Qiao, Q. Wang, D. Lei, X. Shi, Q. Zhang, C. Huang, A. Liu, G. He and F. Zhang, *J. Mater. Chem. A*, 2022, **10**, 11702-11711.

6 L. Zhang, Y. Liu, Z. Zhao, P. Jiang, T. Zhang, M. Li, S. Pan, T. Tang, T. Wu, P. Liu, Y. Hou and H. Lu, *ACS Nano*, 2020, **14**, 8495-8507.

7 Y. J. Liu, D. H. Hong, M. Q. Chen, Z. Su, Y. F. Gao, Y. Y. Zhang and D. H. Long, *Chem. Eng. J.*, 2022, **430**, 132714.

8 Y. J. Liu, D. H. Hong, M. Q. Chen, Z. Su, Y. F. Gao, Y. Y. Zhang and D. H. Long, *ACS Appl. Mater. Interfaces*, 2021, **13**, 35008-35018.

9 Y. Kong, X. Ao, X. Huang, J. Bai, S. Zhao, J. Zhang and B. Tian, *Adv. Sci.*, 2022, **9**, 2105538.

10 W. L. Cai, G. R. Li, K. L. Zhang, G. N. Xiao, C. Wang, K. F. Ye, Z. W. Chen, Y. C. Zhu and Y. T. Qian, *Adv. Funct. Mater.*, 2018, **28**, 1704865.

11 C. Song, W. Zhang, Q. Jin, Y. Zhao, Y. Zhang, X. Wang and Z. Bakenov, *Journal of Materials Science & Technology*, 2022, **119**, 45-52.

12 H. H. Li, H. Q. Chen, Y. X. Chen, G. Y. Bai, M. J. Zhang, S. S. Xie and K. L. Zhuo, *Inorg. Chem. Front.*, 2021, **8**, 4341-4348.

13 S. Fan, S. Z. Huang, M. E. Pam, S. Chen, Q. Y. Wu, J. P. Hu, Y. Wang, L. K. Ang, C.

C. Yan, Y. M. Shi and H. Y. Yang, *Small*, 2019, **15**, 1906132.

14 W. Xiaoxiao, D. Nanping, L. Yarong, W. Liying, W. Hao, L. Yanan, C. Bowen and K. Weimin, *Chem. Eng. J.*, 2022, **450**, 138191.

15 H. Li, P. Shi, L. Wang, T. Yan, T. Guo, X. Xia, C. Chen, J. Mao, D. Sun and L. Zhang, *Angew. Chem. Int. Ed.*, 2023, **62**, e202216286.